J. theor. Biol. (2003) **221,** 491–511
doi:10.1006/jtbi.2003.3200, available online at http://www.idealibrary.com on IDEAL®

A Robust Numerical Algorithm for Studying Biomolecular Transport Processes

HONGYUN WANG†, CHARLES S. PESKIN‡ AND TIMOTHY C. ELSTON*§

†*Department of Applied Mathematics and Statistics, University of California, Santa Cruz, CA* 95064, *U.S.A.* ‡*Courant Institute of Mathematical Sciences, New York University*, 251 *Mercer St., New York, NY* 10012, *U.S.A. and* §*Department of Mathematics, University of North Carolina at Chapel Hill, Chapel Hill, NC* 27599-3250, *U.S.A.*

(*Received on* 19 *August* 2002, *Accepted in revised form on* 28 *October* 2002)

We present a numerical algorithm that is well suited for the study of biomolecular transport processes. In the algorithm a continuous Markov process is discretized as a jump process and the jump rates are derived from local solutions of the continuous system. Consequently, the algorithm has two advantages over standard numerical methods: (1) it preserves detailed balance for equilibrium processes, (2) it is able to handle discontinuous potentials. The formulation of the algorithm also allows us to calculate the effective diffusion coefficient or, equivalently, the randomness parameter. We provide several simple examples of how to implement the algorithm. All the MATLAB functions files needed to reproduce the results presented in the article are available from www.amath.unc.edu/Faculty/telston/matlab_functions.

1. Introduction

One way that cells accomplish biomolecular transport is through the use of motor proteins, such as cytoplasmic kinesins and dyneins. Using laser-trapping techniques, the biophysical properties of single motor proteins can now be measured. This, coupled with increased biochemical and structural data for molecular motors, has sparked a renewed interest in the mathematical modeling of motor protein function. In general, mechanistic models of energy transduction in motor proteins must be studied numerically, because analytic solutions to model equations exist only for very simple systems. Here we present a numerical scheme for studying biomolecular transport processes. The method is based on the ideas of Elston & Doering (1996) and Peskin (unpublished). The advantages of our method are that it preserves the property of detailed balance for systems in equilibrium and is capable of handling discontinuous potentials (e.g. sawtooth or ratchet potentials).

We present several examples that illustrate how the algorithm can be implemented. For clarity the examples considered here are very stylized and lack biological detail. However, the algorithm has been successfully used to study ATP synthase (Elston *et al.*, 1998; Wang & Oster 1998) and protein translocation (Elston, 2002). Also, we show how the algorithm can be used to

*Corresponding author. Tel.: +1-919-515-1910; fax: +1-919-515-1909.
E-mail address: hongwang@ams.ucsc.edu (H. Wang), peskin@cims.nyu.edu (C. S. Peskin), elston@amath.unc.edu (T. C. Elston).

0022-5193/03/$35.00

compute the average velocity and effective diffusion coefficient. These quantities are needed to calculate the randomness parameter (Schnitzer & Block, 1995), which has been shown to provide useful information about the mechanochemical cycle of the motor. All the MATLAB function files that are needed to generate the results presented in this manuscript are available from www.amath.unc.edu/Faculty/telston/matlab_functions. The technical details of the algorithm can be found in the numerous Appendices to this article.

2. Description of the Algorithm

Because of the very low Reynolds numbers involved in biomolecular processes, we only consider overdamped dynamics. To illustrate the method, we restrict ourselves to one-dimensional motion. The algorithm is easily generalized to higher dimensions. In the examples provided below, we assume that the diffusion coefficient does not have a spatial dependence. However, in Appendix A, we generalize the algorithm to include the possibility of a spatially dependent diffusion coefficient.

The dynamics of a one-dimensional Brownian particle subject to a potential is described by the following Langevin equation:

$$\zeta \frac{\mathrm{d}x}{\mathrm{d}t} = -\frac{\partial \phi(x)}{\partial x} + \sqrt{2\zeta k_B T}\tilde{f}(t), \tag{1}$$

where ζ is the friction coefficient, x is the position of the particle, $\phi(x)$ is the potential energy, k_B is the Boltzmann constant and T is the absolute temperature. $\tilde{f}(t)$ represents a Gaussian white-noise stochastic process. At physiological temperatures $k_B T \approx 4.2$ pN nm. The friction coefficient is related to the diffusion coefficient, D, through the Einstein relation $D = k_B T/\zeta$. Typical values of D for proteins in solution are $\approx 10^7$ nm^2 s^{-1}. The probability density $\rho(x,t)$ for x evolves according to the Fokker–Planck equation

$$\frac{\partial \rho(x,t)}{\partial t} = D\frac{\partial}{\partial x}\left(\frac{1}{k_B T}\frac{\partial \phi(x)}{\partial x}\rho(x,t) + \frac{\partial}{\partial x}\rho(x,t)\right). \tag{2}$$

Sample paths of the process can be generated by using an Euler method to approximate eqn (1). That is,

$$x(t+\Delta t) = x(t) - \Delta t\frac{1}{\zeta}\frac{\partial \phi(x)}{\partial x} + \sqrt{2D}\Delta W(\Delta t), \tag{3}$$

where the increments of the Wiener process $\Delta W(\Delta t)$ are independent normally distributed random variables with mean zero and standard deviation $\sqrt{\Delta t}$. While eqn (3) is easy to implement, it has the disadvantage of not preserving the property detailed balance in certain situations (Elston & Doering, 1996).

We present an alternative approach to the problem that provides a method for generating sample paths that respect detailed balance and provides an efficient method for solving eqn (2). The basic idea is to produce a finite differencing of eqn (2) that can be interpreted as a spatially discrete Markov chain (see Fig. 1). That is, we consider a set of discrete sites $x_n = x_0 + n\Delta x$ and look for a finite differencing of the form

$$\begin{aligned}\frac{\mathrm{d}p_n}{\mathrm{d}t} &= -(B_{n-1/2} + F_{n+1/2})p_n + F_{n-1/2}p_{n-1} \\ &\quad + B_{n+1/2}p_{n+1} \\ &= (F_{n-1/2}p_{n-1} - B_{n-1/2}p_n) \\ &\quad - (F_{n+1/2}p_n - B_{n+1/2}p_{n+1}) \\ &= J_{n-1/2} - J_{n+1/2}.\end{aligned} \tag{4}$$

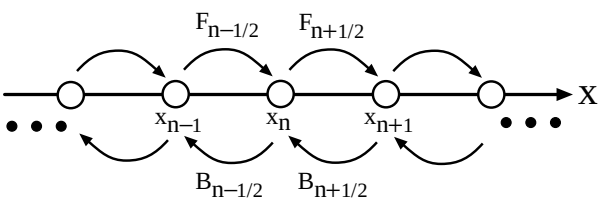

FIG. 1. Our approach to the spatial discretization. The spatially continuous stochastic process [eqns (1) and (2)] is approximated by a spatially discrete jump process. The system is restricted to a set of discrete sites $x_n = x_0 + n\Delta x$ and is only allowed to jump to the neighboring sites. This is a fairly general framework for the spatial discretization. Even the standard central difference method can be cast into this form (see Appendix F).

Here $p_n(t)$ is the probability of finding the motor at site x_n at time t. Since the site x_n represents the interval $(x_{n-1/2}, x_{n+1/2})$, $p_n(t)$ satisfies

$$p_n(t) \approx \int_{x_n-\Delta x/2}^{x_n+\Delta x/2} \rho(x,t)\,\mathrm{d}x \approx \rho(x_n,t)\Delta x. \quad (5)$$

$F_{n+1/2}$ and $B_{n+1/2}$ are, respectively, the forward and backward transition rates between sites x_n and x_{n+1}. $J_{n+1/2}$ is the net probability flux between sites x_n and x_{n+1}. By definition detailed balance requires that at thermodynamic equilibrium the probability flux is identically zero. That is,

$$J_{n+1/2} = F_{n+1/2}\rho_{eq}(x_n)\Delta x - B_{n+1/2}\rho_{eq}(x_{n+1})\Delta x = 0 \quad (6)$$

for all n. $\rho_{eq}(x)$ is the equilibrium solution of eqn (2) and is given by the Boltzmann distribution

$$\rho_{eq}(x) \propto \exp\left(\frac{-\phi(x)}{k_B T}\right). \quad (7)$$

This places a constraint on the transition rates

$$\frac{F_{n+1/2}}{B_{n+1/2}} = \frac{\rho_{eq}(x_{n+1})}{\rho_{eq}(x_n)} = \exp\left(\frac{-\Delta\phi_{n+1/2}}{k_B T}\right), \quad (8)$$

where $\Delta\phi_{n+1/2}$ is defined to be

$$\Delta\phi_{n+1/2} = \phi(x_{n+1}) - \phi(x_n). \quad (9)$$

In Appendix A, we use local approximate solutions to eqn (2) to derive the following formulae for the jump rates:

$$F_{n+1/2} = \frac{D}{(\Delta x)^2}\frac{\Delta\phi_{n+1/2}/k_B T}{\exp(\Delta\phi_{n+1/2}/k_B T) - 1}, \quad (10)$$

$$B_{n+1/2} = \frac{D}{(\Delta x)^2}\frac{-\Delta\phi_{n+1/2}/k_B T}{\exp(-\Delta\phi_{n+1/2}/k_B T) - 1}. \quad (11)$$

Noting the identity, $(1 - \mathrm{e}^{-a})/(\mathrm{e}^{a} - 1) = \mathrm{e}^{-a}$, it is easy to verify that eqns (10) and (11) satisfy eqn (8). Equation (4) can be written in matrix form as

$$\frac{\mathrm{d}\mathbf{p}}{\mathrm{d}t} = \mathbf{L}\mathbf{p}, \quad (12)$$

where $\mathbf{L}$ is a tridiagonal matrix with elements of the form

$$L_{n,n} = -(F_{n+1/2} + B_{n-1/2}), \quad (13)$$

$$L_{n-1,n} = B_{n-1/2}, \quad (14)$$

$$L_{n+1,n} = F_{n+1/2}. \quad (15)$$

3. Applications

3.1. THE TWO-STATE RATCHET

A mathematical description of motor proteins requires not only keeping track of the motor's position, but also its chemical state. In general, reaction cycles are complicated with many intermediate steps. However, we will treat the case in which the motor exists in two chemical states. Steady-state numerical analysis of the flux and force generated by such systems is described by Chiu & Peskin (2002). For more biologically realistic treatments of ATP synthase and the bacterial flagellar motor, we refer the reader to the literature (Elston & Oster, 1998; Elston *et al.*, 1998; Wang & Oster, 1998). Theoretical treatments of abstract models can be found in the physics literature (see for example Riemann, 2002). We chose a two-state model, because it is sufficient to illustrate how the algorithm can be applied to systems with multiple chemical states, yet simple enough so that the reader will not get lost in the details. To be concrete, this example can be thought of a model for motor protein moving along a polymer. The motor can be in one of two chemical states, S_1 and S_2. For example, these two states might correspond to the nucleotide-binding site being occupied or empty. The kinetic scheme for this reaction is

$$S_1 \underset{k_{21}(x)}{\overset{k_{12}(x)}{\rightleftharpoons}} S_2, \quad (16)$$

where the rate constants, k_{12} and k_{21}, are assumed to depend on the position of the motor along the polymer. The mechanical forces that the motor experiences are assumed to arise from the potentials $\phi_1(x)$ and $\phi_2(x)$, corresponding to S_1 and S_2, respectively. The diffusion equations

that govern this process are

$$\frac{\partial \rho_1}{\partial t} = D\frac{\partial}{\partial x}\left(\frac{1}{k_B T}\frac{\partial \phi_1}{\partial x}\rho_1 + \frac{\partial}{\partial x}\rho_1\right) - k_{12}\rho_1 + k_{21}\rho_2, \tag{17}$$

$$\frac{\partial \rho_2}{\partial t} = D\frac{\partial}{\partial x}\left(\frac{1}{k_B T}\frac{\partial \phi_2}{\partial x}\rho_2 + \frac{\partial}{\partial x}\rho_2\right) - k_{21}\rho_2 + k_{12}\rho_1. \tag{18}$$

At steady state, the total flux in the spatial dimension

$$\begin{aligned} J = & -D\left(\frac{1}{k_B T}\frac{\partial \phi_1}{\partial x}\rho_1 + \frac{\partial}{\partial x}\rho_1\right) \\ & -D\left(\frac{1}{k_B T}\frac{\partial \phi_2}{\partial x}\rho_2 + \frac{\partial}{\partial x}\rho_2\right) \\ = & j_1 + j_2 \end{aligned} \tag{19}$$

is a constant independent of x. Thermodynamic equilibrium requires that j_1 and j_2 are identically zero and that $k_{12}\rho_1 - k_{21}\rho_2$ (the flux between S_1 and S_2) is identically zero. In this case, the probability densities are proportional to the Boltzmann distributions

$$\rho_i(x,t) \propto \mathrm{e}^{-\phi_i(x)/k_B T} \tag{20}$$

which forces the following constraint on the rates:

$$\frac{k_{12}(x)}{k_{21}(x)} \propto \mathrm{e}^{(\phi_1(x)-\phi_2(x))/k_B T}. \tag{21}$$

If eqn (21) is not obeyed, then in general the system will experience a net flux (i.e. $J \neq 0$). These types of systems have been referred to generically as "flashing" or "correlation" ratchets.

To solve numerically eqns (17) and (18), we use periodic boundary conditions. That is $\rho_i(x + L, t) = \rho_i(x, t)$, where L can be thought of as the repeat length of the polymer track. The grid is chosen so that $x_n = (n - 1/2)L/N$, where N is the number of grid points. The discretized version of the equations is

$$\frac{\mathrm{d}\mathbf{p}}{\mathrm{d}t} = \mathbf{M}\mathbf{p}. \tag{22}$$

$\mathbf{M}$ is a $2N \times 2N$ matrix of the form

$$\mathbf{M} = \begin{pmatrix} \mathbf{L}^{(1)} - \mathbf{K}_{12} & \mathbf{K}_{21} \\ \mathbf{K}_{12} & \mathbf{L}^{(2)} - \mathbf{K}_{21} \end{pmatrix}, \tag{23}$$

where the $\mathbf{L}^{(i)}$ are $N \times N$ matrices evaluated using $\phi_i(x)$ and have similar form as the matrix $\mathbf{L}$ defined by eqns (13–15), except enforcement of the periodic boundary conditions requires that

$$L^{(i)}_{N,1} = B^{(i)}_{1/2}, \tag{24}$$

$$L^{(i)}_{1,N} = F^{(i)}_{N+1/2}. \tag{25}$$

$\mathbf{K}_{12}$ and $\mathbf{K}_{21}$ are $N \times N$ diagonal matrices with the values of the two respective rate constants evaluated at the grid points along the diagonal.

We take the potentials to have the following forms:

$$\phi_1(x) = \frac{2A}{\pi}\left(\sin\left(\frac{2\pi}{L}x\right) - \frac{1}{2}\sin\left(\frac{4\pi}{L}x\right) + \frac{1}{3}\sin\left(\frac{6\pi}{L}x\right)\right), \tag{26}$$

$$\phi_2(x) = 0. \tag{27}$$

The right-hand side of $\phi_1(x)$ is the first three terms in a Fourier expansion of a sawtooth potential of period L and amplitude A. While this simple system should not be taken seriously as a model of motor protein function, it does have some similarities with dynein. It has been observed that at high ADP levels, dynein is able to diffuse along the microtubule (Vale *et al.*, 1989). This would correspond to the system being in S_2 ($\phi_2 = 0$). Therefore, we shall use the experimentally measure value of the diffusion coefficient $D = 9 \times 10^3$ nm^2 s^{-1}, which is considerably less than what would be expected for a dynein molecule in solution ($\approx 10^7$ nm^2 s^{-1}). S_1 corresponds to the dynein heads being empty or occupied with ATP, in which case the heads interact strongly with microtubules. The

potential $\phi_1(x)$ is periodic, but spatially asymmetric. We take $L = 8$ nm to correspond to the repeat length of the microtubule. Under physiological conditions 1 ATP molecule is worth approximately $20k_BT$. Therefore, we will take $A = 10k_BT$.

Equation (22) represents a continuous time Markov chain. Exact sample paths for this process can be generated through use of the Gillespie method (Gillespie, 1977). These sample paths are approximations to the continuous process defined by eqns (17) and (18) and become exact in the limit $\Delta x \to 0$. The advantage of this method over the Euler method, eqn (3), is that this method preserves detailed balance for equilibrium processes (Elston & Doering, 1995; Mogilner *et al.*, 2002). The parameter values needed to reproduce the results presented throughout this article are listed in the corresponding figure captions. Figure 2(a) shows an example of a sample path generated when eqn (21) is obeyed. In this case, the system is in equilibrium and no net flux is observed. Figure 3(a) is a sample path generated when the transition rates are taken

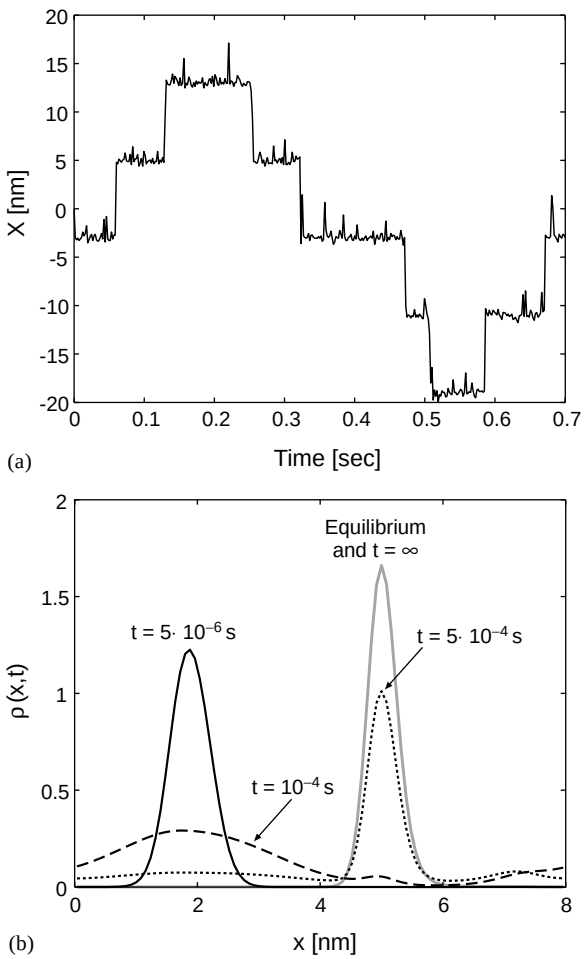

FIG. 2. (A) A sample path of the process generated using sample_paths.m. The transition rates were chosen to satisfy eqn (21), the condition for detailed balance. Therefore, no net drift is seen. (B) Evolution of the marginal density for x generated with flash_int.m. The gray solid line is the equilibrium density, eqn (28). In both panels $k_{12} = 8400 \exp(\phi_1(x)/k_BT)\ \mathrm{s}^{-1}$ and $k_{21} = 8400 \exp(\phi_2(x)/k_BT)\ \mathrm{s}^{-1}$, and the parameter values are $L = 8$ nm, $D = 9 \times 10^3\ \mathrm{nm}^2\ \mathrm{s}^{-1}$, $k_BT = 4.2$ pN nm, $A = 10k_BT$, $N = 100$, $\Delta x = L/N = 0.08$ nm, and $\Delta t = 7.1 \times 10^{-7}$ s. The initial condition for $\mathbf{p}$ was $p_n = 0$ for $n \neq N/4$ and $p_{N/4} = 1$.

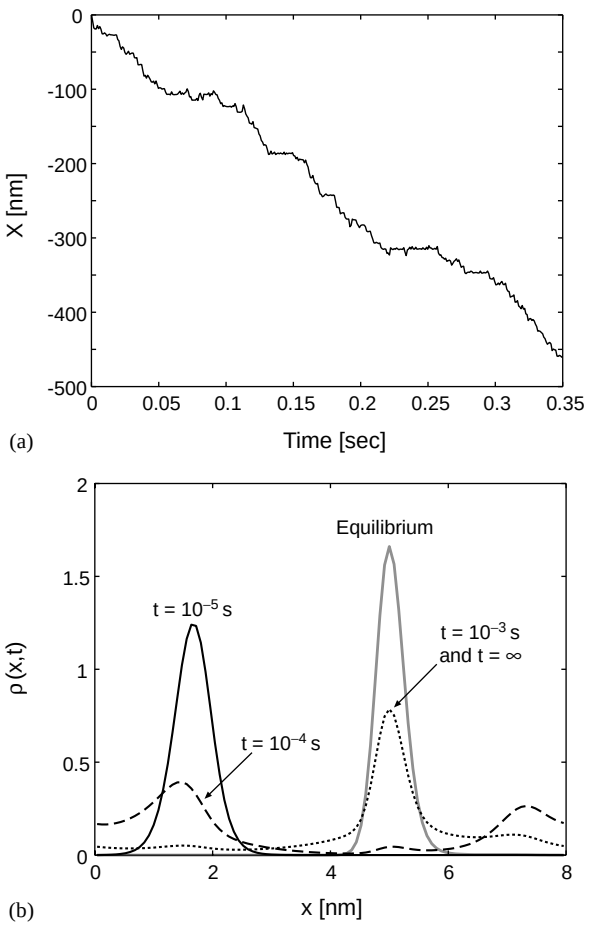

FIG. 3. The same as Fig. 1, except $k_{12} = k_{21} = 8400\ \mathrm{s}^{-1}$. (A) A sample path of the process generated by sampl_paths.m. Because eqn (21) is not satisfied a clear negative drift is seen. (B) Evolution of the marginal density for x. For reference the equilibrium distribution is again plotted as the gray line. Notice that the steady state deviates from equilibrium because eqn (21) is not satisfied.

as $k_{12} = k_{21} = 8.1 \times 10^3\ \mathrm{s}^{-1}$. Because eqn (21) is not satisfied, a persistent drifting in the negative direction can be seen in this figure. The MATLAB function samp_paths.m was used to generate both samples paths (see www.amath.unc.edu/Faculty/telston/matlab_functions).

We next use the algorithm to study the time evolution of probability densities. The MATLAB function flash_int.m numerically solves eqns (17) and (18) with periodic boundary conditions. The function uses the Crank–Nicholson algorithm to integrate numerically eqn (22). Figure 2(b) shows the marginal density $\rho(x) = \rho_1(x) + \rho_2(x)$ at various times when eqn (21) is obeyed. Also shown is the marginal equilibrium distribution

$$\rho_{eq}(x) = \frac{q_2 \mathrm{e}^{-\phi_1(x)/k_B T} + q_1 \mathrm{e}^{-\phi_2(x)/k_B T}}{q_2 Y_1 + q_1 Y_2}, \quad (28)$$

where

$$q_i = \int_0^L k_{ij}(x) \mathrm{e}^{-\phi_i(x)/k_B T}\, \mathrm{d}x, \quad (29)$$

$$Y_i = \int_0^L \mathrm{e}^{-\phi_i(x)/k_B T}\, \mathrm{d}x. \quad (30)$$

Figure 3(b) shows the evolution of the marginal density for the case $k_{12}(x) = k_{21}(x) = 8.1 \times 10^3\ \mathrm{s}^{-1}$. At $t = 10^{-3}$ s, the system has essentially reached steady state. For reference the equilibrium distribution is also shown in this figure. Because eqn (21) is not satisfied the steady state deviates from equilibrium and produces a steady-state flux. In Section 4, we show how to compute the average velocity and effective diffusion coefficient of the system.

3.2. THE PERFECT BROWNIAN RATCHET

In this section, we consider the perfect Brownian ratchet. The motivation for this example is that it allows us to introduce an absorbing boundary condition. A Brownian ratchet refers to a diffusive transport process in which a Brownian particle is driven by ratcheting boundaries placed at $x = 0, \pm L, \pm 2L, \ldots$. These boundaries correspond to large free energy drops caused by chemical reactions. A perfect ratchet is an idealization in the limit that the chemical reaction is much faster than the diffusion of the particle and that the free energy drop caused by the chemical reaction is much larger than the thermal energy ($k_B T$). When the particle goes over a perfect ratchet boundary from the left, the large free energy drop prevents it from going back. Thus, a perfect ratchet boundary acts as an absorbing boundary when approached from the left; it acts as a reflecting boundary when approached from the right. The loaded perfect ratchet refers to the case in which a constant load force is also applied to the Brownian particle.

Let x be the position of the particle relative to the last ratchet boundary it crossed ($0 \leqslant x \leqslant L$). Let f be the constant load force on the particle ($f < 0$ if it is against the ratchet). The evolution of the probability density of the loaded perfect ratchet is governed by the equation

$$\frac{\partial \rho}{\partial t} = \frac{\partial}{\partial x}\left(D \frac{-f}{k_B T} \rho + D \frac{\partial \rho}{\partial x} \right) \quad (31)$$

with boundary conditions

$$\rho(L, t) = 0, \quad (32)$$

$$D\left(\frac{f}{k_B T} \rho - \frac{\partial \rho}{\partial x} \right)\Big|_{x=0} = D\left(\frac{f}{k_B T} \rho - \frac{\partial \rho}{\partial x} \right)\Big|_{x=L}. \quad (33)$$

Equation (32) is an absorbing boundary condition. In Appendix C, we derive the jump rates at absorbing boundaries for the spatial discretization

$$F^{absorb}_{N+1/2} = \frac{D}{(\Delta x)^2} \frac{(-\alpha)^2}{\exp(-\alpha) - 1 - (-\alpha)},$$
$$\alpha = -\frac{\phi_N - \phi_{N-1}}{k_B T}. \quad (34)$$

The discretized equation at $x = L$ (absorbing boundary) is then given by

$$\frac{\mathrm{d}p_N}{\mathrm{d}t} = -(B_{N-1/2} + F^{absorb}_{N+1/2}) p_N + F_{N-1/2} p_{N-1}. \quad (35)$$

The exact average velocity of the perfect Brownian ratchet is

$$v = \frac{D}{L}\frac{\alpha_L^2}{\exp(-\alpha_L) - 1 + \alpha_L}, \quad \alpha_L = \frac{fL}{k_B T}. \tag{36}$$

A derivation of this result is provided in Appendix D. In Appendix D, we also show that when the boundary condition given by eqn (34) is used, the numerical scheme reproduces the exact steady-state solution for the perfect Brownian ratchet, and, therefore, the exact average velocity given in eqn (36).

4. The Mean Velocity and Effective Diffusion Coefficient

Many motor proteins process along polymer filaments. With the advent of laser traps it is now possible to track the position of single molecules. This allows the molecule's mean position $\langle x(t)\rangle$ to be measured as function of time, as well as the variance in the position $\sigma^2(t) = \langle x(t)^2\rangle - \langle x(t)\rangle^2$. The average velocity of the motor can be computed by

$$v = \lim_{t\to\infty} \frac{\langle x(t)\rangle}{t}. \tag{37}$$

Under fairly general conditions, it can be shown that after long times the variance grows linearly in time (Elston, 2000). That is, for $t \gg 1$

$$\sigma^2(t) = 2D_{eff}t. \tag{38}$$

Schnitzer & Block (1995) have shown that useful information about the chemical cycle that drives the motor's motion can be inferred from the randomness parameter defined as

$$r = \lim_{t\to\infty} \frac{\sigma^2(t)}{\langle x(t)\rangle L} = \frac{2D_{eff}}{vL}, \tag{39}$$

where L is the repeat length of the polymer track on which the motor moves. If the motor is assumed to produce a motor step of length L per reaction cycle, then $1/r$ puts a lower bound on the number of chemical steps per cycle. The case $r = 1$ indicates a Poisson process. That is, there is one rate-limiting chemical step per physical step. As we will show, if the motor can move continuously along the polymer, interpretation of the randomness parameter is not as straightforward.

We now show how our algorithm can be used to compute v and D_{eff}, which are required for calculating r. We start by considering a single tilted periodic potential

$$\phi(x + L) = \phi(x) + \Delta\phi, \tag{40}$$

where $\Delta\phi$ is a constant independent of x. In Example 3, we show how to generalize this method to include flashing ratchets. Note that if $\Delta\phi = 0$, then $\phi(x)$ is periodic with period L, and we expect the mean velocity to be zero. Let j indicate the particular period of the potential in which the motor is located and let y represent the position of the particle within the j-th period. The position of the particle is then given by $x = jL + y$. Let N be the number of grid points per period of the potential, $\Delta y = L/N$. Let $p_n(j,t)$ be the probability that the motor is at $x_n(j) = jL + (n - 1/2)\Delta y$. The resulting master equation for the discrete process is

$$\frac{\mathrm{d}}{\mathrm{d}t}\mathbf{p}(j,t) = \mathbf{L}\mathbf{p}(j,t) + \mathbf{L}_+\mathbf{p}(j-1,t) + \mathbf{L}_-\mathbf{p}(j+1,t), \tag{41}$$

where

$$\mathbf{p}(j,t) = \begin{pmatrix} p_1(j,t) \\ p_2(j,t) \\ \vdots \\ p_N(j,t) \end{pmatrix}. \tag{42}$$

The $N \times N$ matrix $\mathbf{L}$ in eqn (41) is a tridiagonal matrix of the form given in eqns (13–15), and $\mathbf{L}_+$ and $\mathbf{L}_-$ are $N \times N$ matrices whose elements are zero, except for $(L_+)_{1,N} = F_{N+1/2}$ and $(L_-)_{N,1} = B_{1/2}$. In Appendix G, we derive the following expressions for the average velocity and effective diffusion coefficient

$$v = L\sum_{n=1}^{N} [(\mathbf{L}_+ - \mathbf{L}_-)\mathbf{p}^s]_n, \tag{43}$$

$$D_{eff} = \frac{L^2}{2}\sum_{n=1}^{N}[(\mathbf{L}_+ + \mathbf{L}_-)\mathbf{p}^s + 2(\mathbf{L}_+ - \mathbf{L}_-)\mathbf{r}]_n, \quad (44)$$

where $\mathbf{p}^s$ and $\mathbf{r}$ are determined by the equations

$$\mathbf{M}\mathbf{p}^s = (\mathbf{L} + \mathbf{L}_- + \mathbf{L}_+)\mathbf{p}^s = 0, \quad (45)$$

$$\mathbf{M}\mathbf{r} = \left(\sum_{n=1}^{N}[(\mathbf{L}_+ - \mathbf{L}_-)\mathbf{p}^s]_n - (\mathbf{L}_+ - \mathbf{L}_-)\right)\mathbf{p}^s \quad (46)$$

subject to the constraints

$$\sum_{n=1}^{N} p_n^s = 1 \quad \text{and} \quad \sum_{n=1}^{N} r_n = 0. \quad (47)$$

The MATLAB function avgv_deff.m numerically solves eqns (45) and (46). The function file flash_deff.m solves the analogous equations for the flashing ratchet.

4.1. EXAMPLE I—THE CORRAL AND TRAPPING MODELS

We begin by considering two simple and related models for which an analytic expression for the effective diffusion can be found. The models were inspired by studies on the dynamics of membrane bound proteins that interact with the cytoskeleton (Sako & Kusumi, 1995). For simplicity, we assume that the membrane bound protein can only diffuse in one dimension. Next, we assume that the cytoskeleton filaments form a regular lattice with the distance between fibers being L. Figure 4(a) shows the corral model. In this model, the filaments represent barriers which must be surmounted by the diffusing protein. The barriers are characterized by their height ΔG and width δ. Figure 4(b) shows the trapping model. In this case, the cytoskeleton fibers represent binding sites for the diffusing molecule. The two different models are related by the transformation $\Delta G \to -\Delta G$. The analytic expression of the effective diffusion coefficient can be found using the method described by Elston (2002). It turns out that for both models, the effective diffusion coefficient is

$$D_{eff} = \frac{D}{1 + 4\sinh^2(\Delta G/2k_BT)(\delta/L)(1-\delta/L)}. \quad (48)$$

Figure 5 shows a plot of D_{eff}/D vs. δ/L for various values of ΔG. The lines correspond to eqn (48) and the $\times$'s are the numerical results.

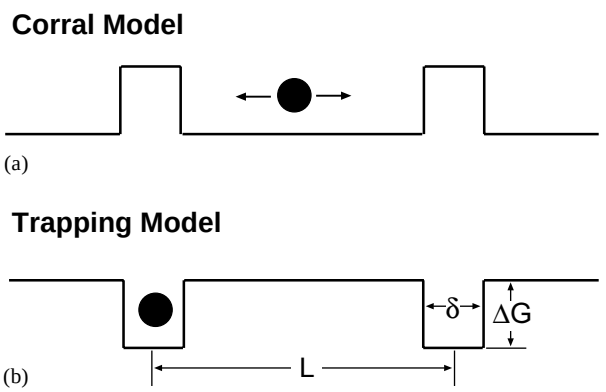

FIG. 4. The corral and trapping models. Both models are characterized by the repeat distance L, the height of the potential barrier ΔG, and δ the width of the barrier (or well). (A) In the corral model the Brownian particle spends most of its time trapped between two potential barriers that require thermal activation to surmount. (B) In the trapping model, the Brownian particle spends most of its time trapped in a potential well.

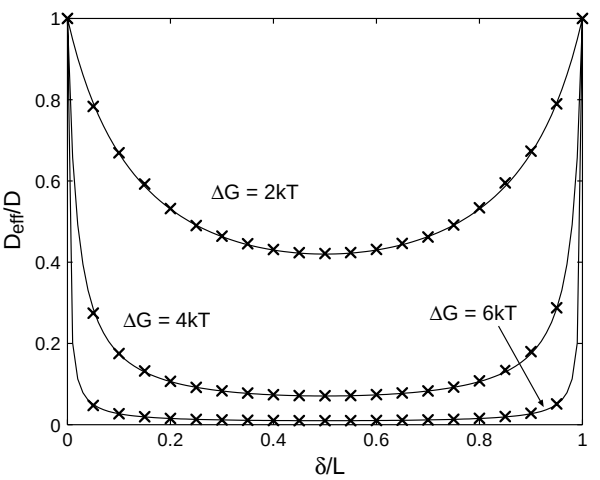

FIG. 5. The ratio D_{eff}/D as a function of δ/L for various values of ΔG. The solid lines are the exact values from eqn (48). The $\times$'s are the numerical results produced using avgv_deff.m with $L = 1$, $D = 1$, and $k_BT = 1$, in arbitrary units, and $N = 100$.

4.2. EXAMPLE II—TILTED SINE POTENTIAL

In this example we consider a potential of the form

$$\phi(x) = A \sin\left(\frac{2\pi}{L}x\right) - fx. \tag{49}$$

If $f = 0$, the effective diffusion coefficient can be approximated as

$$D_{eff} = D\frac{2\pi A}{k_B T} e^{-2A/k_B T}. \tag{50}$$

The above expression is based on the Krammers' approximation and is valid when $A \gg k_B T$. Figure 6 shows a plot of $\ln(D_{eff}/D)$ vs. A. The solid line is the numerical results and the dotted line is the results using eqn (50).

Figure 7(a) is a plot of D_{eff}/D vs. f for various values of A. Notice that for this case D_{eff} can be larger than D. Figure 7(b) is a plot of the randomness parameter vs. f. Notice that there is an intermediate range of values of f for which the randomness parameter is approximately 1. This corresponds to the region in which the Krammers' approximation is valid and the force is strong enough that forward transitions over the potential barrier are greatly favored over backward transitions. That is, the process is essentially Poisson. When the force becomes small and backward transition becomes nearly as probable as forward, the randomness parameter becomes large. On the other hand, as the force becomes large, the particle does not feel the potential and the randomness parameter goes to zero.

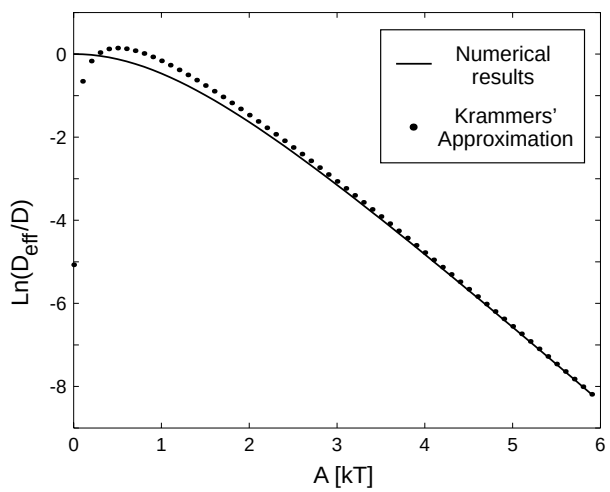

FIG. 6. The ratio D_{eff}/D as a function of A using a sine potential. The solid line is the numerical result using avgv_deff.m with $L = 1$, $D = 1$, and $k_B T = 1$, in arbitrary units, and $N = 100$. The dotted line is the Kramers' approximation, which is valid in the limit $A \gg k_B T$.

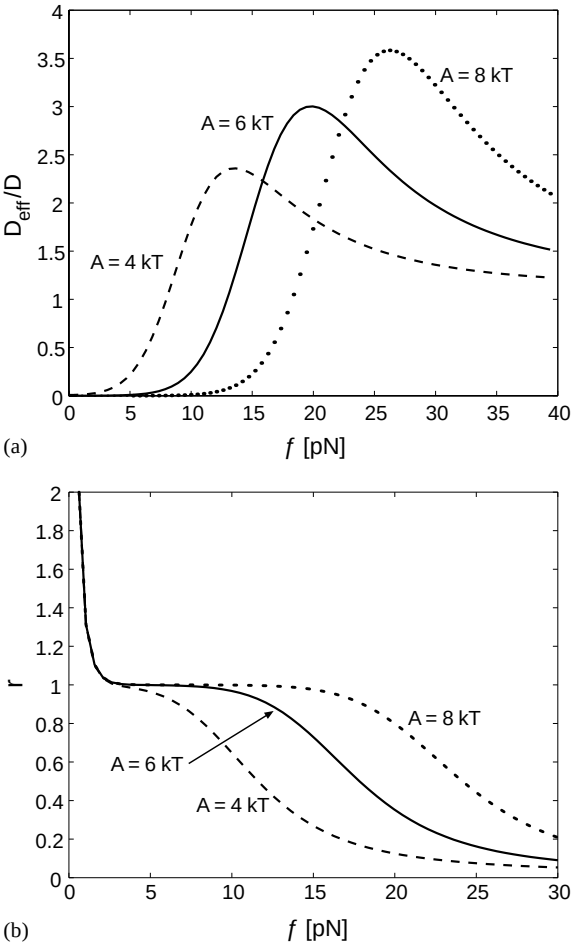

FIG. 7. Numerical results for the titled sine potential using avgv_deff.m. (A) the ratio D_{eff}/D as a function of the applied force f for various values of the amplitude A. In this figure $L = 8$ nm, $D = 9 \times 10^3$ nm^2 s^{-1}, $k_B T = 4.2$ pN nm, $A = 10 k_B T$, and $N = 100$. Note that for this system D_{eff} can be larger than D. (B) The randomness parameter as a function of f using the parameters as in panel A. The region where $r \approx 1$ indicates that the system is behaving like a Poisson process. This region expands as A is increased.

4.3. EXAMPLE III—THE FLASHING RATCHET

In this example we compute the average velocity, effective diffusion coefficient and randomness parameter of the flashing ratchet

considered in Section 3. For this case, the matrices in eqn (41) are $2N \times 2N$ insteady of $N \times N$ because the system has two chemical states. Figures 8(a) and (b) show the average velocity and effective diffusion coefficient, respectively, for various values of A as a function of $\ln(k)$, where $k = k_{12}(x) = k_{21}(x)$. The average velocity has a maximum at around $k = 8400\ \mathrm{s}^{-1}$ and goes to zero as $k \to \infty$ and $k \to 0$. This behavior is easy to understand. Each potential is periodic and cannot produce any net drift by itself. The net drift is produced by the transitions between the two potentials. In the limit of very slow transitions, the net drift is very slow (the amount of net drift per transition cycle actually attains the maximum at infinitesimal slow transitions, not shown in the figure). At the other extreme of very fast transitions, the particles feel the average of the two potentials, which is periodic and produces no net drift. The effective diffusion coefficient also goes through a maximum at roughly the same switching rate as the average velocity. Figure 8(c) shows the randomness parameter plotted as a function of $\ln(k)$. Surprisingly, the randomness parameter is less than 1 for certain parameter values. This indicates the model is behaving less randomly than a Poisson process. For the case with $A = 10k_BT$, the minimum value of r is around 0.6 and $1/r_{min} = 1.7$. If we were dealing with a discrete process we would assume that there must be at least two rate limiting internal sub-steps in each 8 nm displacement (motor step). The minimum of r is attained at $k \approx 8000\ \mathrm{s}^{-1}$ and the corresponding motor velocity is $v \approx 1200\ \mathrm{nm\ s}^{-1}$ (see the figure). The average number of transitions between two potentials per 8 nm displacement is $8000 \times 8/1200 \approx 53$, which is significantly larger than 2.

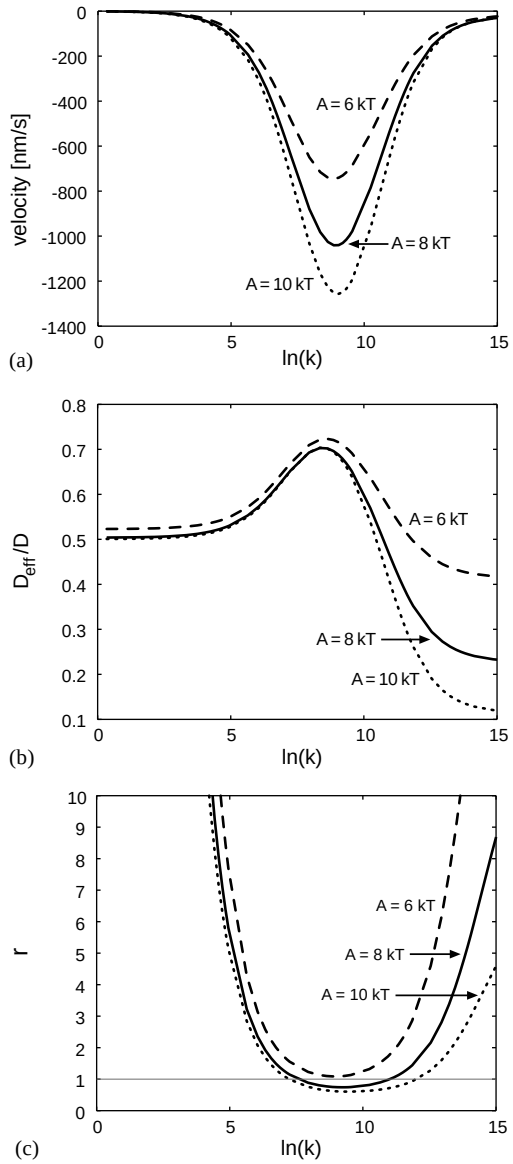

FIG. 8. Numerical results for the flashing ratchet using flash_deff.m. In all the panels $N = 100$, $L = 8$ nm, $D = 9 \times 10^3\ \mathrm{nm^2 s^{-1}}$, $k_BT = 4.2$ pN nm and $k_{12} = k_{21} = k$. (A) The average velocity as a function of $\ln(k)$ for various values of A. The maximum speed occurs around $k = 8400\ \mathrm{s}^{-1}$. (B) The ratio D_{eff}/D as a function $\ln(k)$. The effective diffusion coefficient also has its maximum value around $k = 8400\ \mathrm{s}^{-1}$. (C) The randomness parameter as a function of $\ln(k)$. For large enough values of A, the randomness parameter can be less than 1, indicating the process is less random then a Poisson process.

5. Conclusions

We have presented a numerical algorithm for analysing a class of stochastic processes. The algorithm was developed for studying motor proteins, but can be applied to any overdamped gradient system. In comparison with standard numerical techniques for solving the Fokker–Planck equation and generating sample paths, our numerical method has two advantages: (i) our method preserves the property of detailed balance for systems in equilibrium; (ii) our method works well for non-smooth potentials or even discontinuous potentials while maintaining a second-order accuracy for smooth potentials. Our method was derived by first

approximating a continuous Markov process with a discrete one then calculating the jump rates in the discrete process using local solutions of the continuous system. This approach results in two advantages. The property of detailed balance ensures that our method will not produce an artificial drift velocity while the system is in equilibrium. Thus, the results obtained with our method are physical solutions that do not violate the second law of thermodynamics. It is also very important that the method can handle discontinuous potentials. For example, in models of the F_o motor, the electrostatic potential has a step transition because of the discontinuity in the dielectric coefficient (in water the dielectric coefficient = 80 and in membrane the dielectric coefficient = 3). These two properties of our method make it ideal for studying protein motors and biological transport processes.

Because our method approximates a continuous Markov process with a discrete one, it is also well suited for computing the effective diffusion coefficient. In elegant analyses, Kolomeisky & Fisher (2000a) and Kolomeisky (2001) extended the work of Derrida (1983) and derived exact expressions for the mean velocity and effective diffusion coefficient for discrete Markov chains. Their results are directly applicable to our method. However, the analytic expressions tend to become unwieldy quickly as the complexity of the system increases. Therefore, we have derived a set of linear equations that govern the mean velocity and effective diffusion coefficient. These equations are then solved numerically, which can be done easily using MATLAB.

The randomness parameter, which is defined in terms of the effective diffusion coefficient and average velocity, has a simple interpretation for sequential Markov processes with at least one irreversible step: $1/r$ provides a lower bound for the number of rate-limiting chemical steps per motor step. However, the meaning of the randomness parameter is not clear for more complex processes. For example, Kolomeisky & Fisher (2000b) studied stochastic processes that have non-Markov waiting time distributions and branches. In our study, we have shown that if the motor and track do not interact strongly enough to justify a sequential Markov processes with at least one irreversible step, then interpretation of the randomness parameter is not as straightforward. Therefore, inferences drawn from studying this parameter should be made carefully.

Finally, we note that our algorithm has been successfully used to compute first passage time densities for models of post-translational translocation (Elston, 2002). The details of how to use the algorithm to compute first passage time densities can be found in Chapters 12 and 13 of *Computational Cell Biology* (2002).

All three authors are indebted to George Oster for introducing them to each other, and to the interesting class of problems considered here. H. Wang was supported by NSF grant DMS-0077971. C. Peskin was supported by NIH Grant R01 GM59875-01A1. T. Elston was supported by DARPA grant F30602-01-2-0579 and NSF grant DMS-0075821.

REFERENCES

Chiu, C. & Peskin, C. S. (2002). Numerical analysis of the flux and force generated by a correlation ratchet mechanism. *J. Math. Biol.* **44,** 479–501.

Derrida, B. (1983). Velocity and diffusion constant of a periodic one-dimensional hopping model. *J. Stat. Phys.* **31,** 433–450.

Dimroth, P., Wang, H., Grabe, M. & Oster, G. (1999). Energy transduction in the sodium F-ATPase of *Propionigenium modestum*. *Proc. Natl. Acad. Sci. U.S.A.* **96,** 4924–4929.

Elston, T. (2000). A macroscopic description of biomolecular transport. *J. Math. Biol.* **41,** 189–206.

Elston, T. (2002). The Brownian ratchet and power stroke models for post-translational translocation into the endoplasmic reticulum. *Biophys. J.* **82,** 1239–1253.

Elston, T. & Doering, C. (1996). Numerical and analytical studies of nonequilibrium fluctuation induced transport processes. *J. Stat. Phys.* **83,** 359–383.

Elston, T. & Oster, G. (1997). Protein turbines I: the bacterial flagellar motor. *Biophys. J.* **73,** 703–721.

Elston, T., Wang, H. & Oster, G. (1998). Energy transduction in ATP synthase. *Nature* **391,** 510–513.

Gillespie, D. (1977). Exact stochastic simulation of coupled chemical reactions. *J. Phys. Chem.* **81,** 2340–2361.

Kolomeisky, A. (2001). Exact results for parallel-chain kinetic models of biological transport. *J. Chem. Phys.* **115,** 7253–7259.

Kolomeisky, A. & Fisher, M. (2000a). Periodic sequential kinetic models with jumping, branching and deaths. *Physica* **A279,** 1–20.

Kolomeisky, A. & Fisher, M. (2000b). Extended kinetic models with waiting-time distributions: exact results. *J. Chem. Phys.* **113,** 10867–10877.

Mogilner, A., Elston, T., Wang, H. & Oster, G. (2002). In: *Computational Cell Biology* (Fall, C., Marland, E.,

Wagner, J. & Tyson, J. eds), Chapters 12–13. Berlin: Springer-Verlag.
Peskin, C. & Oster, G. (1995). Coordinated hydrolysis explains the mechanical behavior of kinesin. *Biophys. J.* **68,** 202s–211s.
Reimann, P. (2002). Brownian motors: noisy transport far from equilibrium. *Phys. Rep.* **361,** 57–265
Roe, P. (1981). Approximate Riemann solvers, parameter vectors and difference schemes. *J. Comput. Phys.* **43,** 357–372.
Sako, Y. & Kusumi, A. (1995). Barriers for laterial diffusion of transferrin receptor in the plasma membrane as characterized by receptor dragging by laser tweezers: fence versus tether. *J. Cell Biol.* **129,** 1559–1574.
Schnitzer, M. & Block, S. (1995). Statistical kinetics of processive enzymes. *Cold Spring Harbor Symposium on Quantum Biology* **60,** 793–802.
Vale, R., Soll, D. & Gibbons, I. (1989). One-dimensional diffusion of microtubules bound to flagellar dynein. *Cell* **59,** 915–925.
Wang, H. & Oster, G. (1998). Energy transduction in the F1 motor of ATP synthase. *Nature* **396,** 279–282.

Appendix A

A.1. Derivation of the Numerical Algorithm

A.1.1. *Constant Diffusion Coefficient*

In this appendix, we derive the jump rates using local approximate solutions of the diffusion equation. This approach is similar to the one used to derive the Godunov-type methods for solving conservation laws, which are constructed based on local approximate solutions to the Remiann problem (Roe, 1981).

The diffusion equation for the process is

$$\frac{\partial \rho}{\partial t} = D\frac{\partial}{\partial x}\left(\frac{\phi'(x)}{k_B T}\rho + \frac{\partial \rho}{\partial x}\right). \tag{A.1}$$

In the spatial discretization formulated in eqn (4), the net probability flux from x_n to x_{n+1} is

$$J_{n+1/2} = F_{n+1/2}p_n - B_{n+1/2}p_{n+1}. \tag{A.2}$$

To derive the jump rates, we calculate the net probability flux based on local approximate solutions of eqn (A.1). We first approximate $\phi'(x)$ in the interval $(x_{n-1/2}, x_{n+3/2})$ by a constant. Thus, eqn (A.1) in the interval $(x_{n-1/2}, x_{n+3/2})$ is approximated by

$$\frac{\partial \rho}{\partial t} = \frac{\partial}{\partial x}\left(-D\frac{f}{k_B T}\rho + D\frac{\partial \rho}{\partial x}\right),$$

$$f = -\frac{\Delta\phi_{n+1/2}}{\Delta x},$$

$$\Delta\phi_{n+1/2} = \phi(x_{n+1}) - \phi(x_n). \tag{A.3}$$

Next, we assume that at any given time, $\rho(x, t)$ in the interval $(x_{n-1/2}, x_{n+3/2})$ is approximately at steady state. This assumption is valid, because at small length scales diffusion is the dominant effect. The time-scale for a particle with diffusion coefficient D to diffuse a distance Δx is $\Delta t_{diff} = (\Delta x)^2/2D$, which is proportional to $(\Delta x)^2$. The time-scale for a flow with velocity v to travel a distance of Δx is $\Delta t_{flow} = \Delta x/v$, which is proportional to Δx. For small Δx, $\Delta t_{diff} \ll \Delta t_{flow}$. At small length scales, diffusion relaxes the system to steady state immediately after it is disturbed by the flow. Thus, at any given time, the local structure of the solution is given approximately by the steady-state solution.

We can make a translational transformation to shift $x_{n-1/2}$ to $-\Delta x$. So without the loss of generality, we consider the special case where $(x_{n-1/2}, x_{n+3/2}) = (-\Delta x, \Delta x)$. We set the left-hand side of eqn (A.3) to zero and solve the resulting ordinary differential equation in the interval $(-\Delta x, \Delta x)$

$$\frac{\partial}{\partial x}\left(-D\frac{f}{k_B T}\rho + D\frac{\partial \rho}{\partial x}\right) = 0 \tag{A.4}$$

subject to two conditions:

$$\int_{-\Delta x}^{0} \rho(x)\,\mathrm{d}x = p_n, \quad \int_{0}^{\Delta x} \rho(x)\,\mathrm{d}x = p_{n+1}. \tag{A.5}$$

The general solution of eqn (A.4) has the form

$$\rho(x) = c_1 \exp\left(\frac{fx}{k_B T}\right) + c_2. \tag{A.6}$$

Constants c_1 and c_2 are determined from eqn (A.5)

$$c_1 = -\frac{\alpha \exp(\alpha)(p_n - p_{n+1})}{\Delta x\,(\exp(\alpha) - 1)^2},$$

$$c_2 = \frac{\exp(\alpha)p_n - p_{n+1}}{\Delta x\,(\exp(\alpha) - 1)}, \quad \alpha = \frac{f\Delta x}{k_B T}. \tag{A.7}$$

The probability flux is

$$J = D\left(\frac{f}{k_BT}\rho - \frac{\partial\rho}{\partial x}\right)$$
$$= \frac{D}{(\Delta x)^2}\frac{\alpha\exp(\alpha)p_n - \alpha p_{n+1}}{\exp(\alpha)-1}. \quad (A.8)$$

Comparing eqn (A.8) with eqn (A.2), we obtain the jump rates

$$F_{n+1/2} = \frac{D}{(\Delta x)^2}\frac{-\alpha}{\exp(-\alpha)-1},$$

$$B_{n+1/2} = \frac{D}{(\Delta x)^2}\frac{\alpha}{\exp(\alpha)-1},$$

$$\alpha = \frac{f\Delta x}{k_BT} = \frac{-\Delta\phi_{n+1/2}}{k_BT}. \quad (A.9)$$

A.2.1. *Spatially Dependent Diffusion Coefficient*

If the drag coefficient of the particle varies with the particle position ($\zeta = \zeta(x)$), then the diffusion coefficient of the particle is a function of x and the governing equation becomes

$$\frac{\partial\rho}{\partial t} = \frac{\partial}{\partial x}\left(D(x)\frac{\phi'(x)}{k_BT}\rho + D(x)\frac{\partial\rho}{\partial x}\right),$$

$$D(x) = \frac{k_BT}{\zeta(x)}. \quad (A.10)$$

For eqn (A.10), the jump rates in the numerical method can be derived using the same principle as we did for the case of constant diffusion coefficient. Here we discuss separately the case of a continuously varying diffusion coefficient and the case of a step-function diffusion coefficient.

A.2.1.1. *Continuous Diffusion Coefficient*. If the diffusion coefficient is a continuous function of the particle's position, we approximate both $\phi'(x)$ and $D(x)$ in the interval $(x_{n-1/2}, x_{n+3/2})$ by constants. Equation (A.10) in the interval $(x_{n-1/2}, x_{n+3/2})$ is approximated by

$$\frac{\partial\rho}{\partial t} = \frac{\partial}{\partial x}\left(-D_{n+1/2}\frac{f}{k_BT}\rho + D_{n+1/2}\frac{\partial\rho}{\partial x}\right),$$

$$f = -\frac{\Delta\phi_{n+1/2}}{\Delta x},$$

$$D_{n+1/2} = \frac{D(x_n) + D(x_{n+1})}{2}. \quad (A.11)$$

Equation (A.11) is exactly the same as eqn (A.3). Thus the jump rates are given by

$$F_{n+1/2} = \frac{D_{n+1/2}}{(\Delta x)^2}\frac{-\alpha}{\exp(-\alpha)-1},$$

$$B_{n+1/2} = \frac{D_{n+1/2}}{(\Delta x)^2}\frac{\alpha}{\exp(\alpha)-1},$$

$$\alpha = \frac{f\Delta x}{k_BT} = \frac{-\Delta\phi_{n+1/2}}{k_BT}. \quad (A.12)$$

A.2.1.2. *Step-Function Coefficient*. Suppose the diffusion coefficient has a jump at $x_{n+1/2}$. Without loss of generality, we consider the special case where $(x_{n-1/2}, x_{n+3/2}) = (-\Delta x, \Delta x)$. We approximate eqn (A.10) in the interval $(-\Delta x, \Delta x)$ as

$$\frac{\partial\rho}{\partial t} = \frac{\partial}{\partial x}\left(-D(x)\frac{f}{k_BT}\rho + D(x)\frac{\partial\rho}{\partial x}\right), \quad (A.13)$$

$$f = -\frac{\Delta\phi_{n+1/2}}{\Delta x}, \quad D(x) = \begin{cases} D_1 & \text{if } x<0, \\ D_2 & \text{if } x>0. \end{cases}$$

As in the case of constant diffusion coefficient, the jump rates are derived based on the probability flux calculated from the local steady-state solution of eqn (A.13) in $(-\Delta x, \Delta x)$. Setting the left-hand side of eqn (A.13) to zero and integrating with respect to x, we have

$$D(x)\frac{f}{k_BT}\rho - D(x)\frac{\partial\rho}{\partial x} = J. \quad (A.14)$$

Here the probability flux J is an undetermined constant. The general solution of eqn (A.14) is given by

$$\rho(x) = c\exp(ax) + J\frac{(1-\exp(ax))}{a}\begin{cases} \frac{1}{D_1} & \text{if } x<0, \\ \frac{1}{D_2} & \text{if } x>0, \end{cases}$$

$$a = \frac{f}{k_BT}. \quad (A.15)$$

The particular solution we want also satisfies eqn (A.4). Substituting eqn (A.15) into eqn (A.4) and solving for J, we obtain

$$J = \frac{\tilde{D}}{(\Delta x)^2}\frac{\alpha\exp(\alpha)p_n - \alpha p_{n+1}}{(\exp(\alpha)-1) + \Delta D((\exp(\alpha)+1)/2 - (\exp(\alpha)-1)/\alpha)},$$

$$\tilde{D} = \frac{2D_1D_2}{(D_1+D_2)}, \quad \Delta D = \frac{2(D_2-D_1)}{D_1+D_2}, \alpha = \frac{f\Delta x}{k_BT}. \qquad \text{(A.16)}$$

Comparing eqn (A.16) with eqn (A.2), we obtain the jump rates

$$F_{n+1/2} = \frac{\tilde{D}}{(\Delta x)^2}\frac{-\alpha}{(\exp(-\alpha)-1) - \Delta D((\exp(-\alpha)+1)/2 - (\exp(-\alpha)-1)/(-\alpha))},$$

$$B_{n+1/2} = \frac{\tilde{D}}{(\Delta x)^2}\frac{\alpha}{(\exp(\alpha)-1) + \Delta D((\exp(\alpha)+1)/2 - (\exp(\alpha)-1)/\alpha)},$$

$$\tilde{D} = \frac{2D_1D_2}{(D_1+D_2)}, \quad \Delta D = \frac{2(D_2-D_1)}{D_1+D_2}, \alpha = \frac{-\Delta\phi_{n+1/2}}{k_BT}. \qquad \text{(A.17)}$$

Appendix B

B.1. ACCURACY OF THE NUMERICAL METHOD

In this appendix, we show that the numerical method is second-order accurate. We first show that the numerical method has a second-order local truncation error in both time and space (consistency). Then we show that the numerical method is stable (stability). Finally using Lax equivalence theorem, we see that the method converges and the global error is second order both in time and space.

The local truncation error of a numerical method is the error term obtained by substituting the exact solution of the differential equation into the numerical method. Suppose $\rho(x,t)$ is the exact solution of eqn (2) with certain initial and boundary conditions. When we substitute it into the numerical algorithm eqn (4) with $p_n(t) = \rho(x_n,t)$, eqn (4) will not be satisfied exactly. The error term is the local truncation error of numerical algorithm eqn (4). To find the order of the local truncation error of eqn (4), we expand the jump rates $F_{n+1/2}$ and $B_{n+1/2}$ given by eqn (A.9) as functions of α:

$$F_{n+1/2} = \frac{D}{(\Delta x)^2}\frac{-\alpha}{\exp(-\alpha)-1} = \frac{D}{(\Delta x)^2}\left(1 + \frac{1}{2}\alpha + \frac{1}{12}\alpha^2 + 0\alpha^3 + O(\alpha^4)\right), \qquad \text{(B.1)}$$

$$B_{n+1/2} = \frac{D}{(\Delta x)^2}\frac{\alpha}{\exp(\alpha)-1} = \frac{D}{(\Delta x)^2}\left(1 - \frac{1}{2}\alpha + \frac{1}{12}\alpha^2 + 0\alpha^3 + O(\alpha^4)\right),$$

where $\alpha = -\Delta\phi_{j+1/2}/k_BT$. Let ρ_n denote $\rho(x_n,t)$. Using the expansions in eqn (B.1), we get

$$F_{n+1/2}\rho_n - B_{n+1/2}\rho_{n+1} = (F_{n+1/2} - B_{n+1/2})\frac{\rho_{n+1}+\rho_n}{2}$$

$$-\frac{F_{n+1/2}+B_{n+1/2}}{2}(\rho_{n+1}-\rho_n)$$

$$=-\frac{D}{(\Delta x)^2}\left(\frac{\Delta\phi_{n+1/2}}{k_BT}\right)\frac{\rho_{n+1}+\rho_n}{2}$$

$$-\frac{D}{(\Delta x)^2}\left(1+\frac{1}{12}\left(\frac{\Delta\phi_{n+1/2}}{k_BT}\right)^2\right)$$

$$(\rho_{n+1}-\rho_n)+O((\Delta x)^2). \tag{B.2}$$

Expanding $\rho(x,t)$ and $\phi(x)$, we have

$$(F_{n-1/2}\rho_{n-1}-B_{n-1/2}\rho_n)$$

$$-(F_{n+1/2}\rho_n-B_{n+1/2}\rho_{n+1})$$

$$=D\frac{\partial}{\partial x}\left(\frac{\phi'(x)}{k_BT}\rho(x,t)\right)\Big|_{x=x_n}$$

$$+D\frac{\partial^2}{\partial x^2}\rho(x,t)\Big|_{x=x_n}+O((\Delta x)^2). \tag{B.3}$$

Using the differential equation eqn (2), we obtain

$$\frac{\mathrm{d}\rho_n}{\mathrm{d}t}=(F_{n-1/2}\rho_{n-1}-B_{n-1/2}\rho_n)$$

$$-(F_{n+1/2}\rho_n-B_{n+1/2}\rho_{n+1})+O((\Delta x)^2) \tag{B.4}$$

which means the local truncation error of numerical scheme, eqn (4), is second order. The fully discretized method is obtained by applying the Crank–Nicolson discretization in time to eqn (4):

$$\frac{p_j^{n+1}-p_j^n}{\Delta t}$$

$$=\left(F_{j-1/2}\frac{p_{j-1}^{n+1}+p_{j-1}^n}{2}-B_{j-1/2}\frac{p_j^{n+1}+p_j^n}{2}\right)$$

$$-\left(F_{j+1/2}\frac{p_j^{n+1}+p_j^n}{2}-B_{j+1/2}\frac{p_{j+1}^{n+1}+p_{j+1}^n}{2}\right). \tag{B.5}$$

The Crank–Nicolson discretization in time has a second-order local truncation error. Therefore, the local truncation error of eqn (B.5) is second order.

Now we prove that the fully discretized method eqn (B.5) is stable. We consider the case of eqn (B.5) with periodic boundary conditions. The proof can be extended to other situations. We start by introducing the notations

$$\|p^n\|_2^2=\sum_{j=1}^N (p_j^n)^2,\quad p_j^{n+1/2}=\frac{p_j^{n+1}+p_j^n}{2}. \tag{B.6}$$

Multiplying eqn (B.5) by $(p_j^{n+1}+p_j^n)$, summing over index j, applying summation by parts and using periodic boundary conditions, we get

$$\frac{\|p^{n+1}\|_2^2-\|p^n\|_2^2}{\Delta t}$$

$$=-\sum_{j=1}^N 2(F_{j-1/2}p_{j-1}^{n+1/2}-B_{j-1/2}p_j^{n+1/2})$$

$$\times(p_{j-1}^{n+1/2}-p_j^{n+1/2})$$

$$=-\sum_{j=1}^N (F_{j-1/2}+B_{j-1/2})(p_{j-1}^{n+1/2}-p_j^{n+1/2})^2$$

$$-\sum_{j=1}^N (F_{j-1/2}-B_{j-1/2})((p_{j-1}^{n+1/2})^2$$

$$-(p_j^{n+1/2})^2)\equiv I_1+I_2. \tag{B.7}$$

The first term on the right-hand side of eqn (B.7) is non-positive: $I_1\leqslant 0$. Applying summation by parts to the second term yields

$$I_2=\sum_{j=1}^N((B_{j-1/2}-F_{j-1/2})$$

$$-(B_{j+1/2}-F_{j+1/2}))(p_j^{n+1/2})^2. \tag{B.8}$$

Using the expansions in eqn (B.1), we have

$$(B_{j-1/2}-F_{j-1/2})-(B_{j+1/2}-F_{j+1/2})$$

$$=\frac{D}{k_BT}\phi''(x_j)+O((\Delta x)^2). \tag{B.9}$$

When $\phi(x)$ is smooth enough, there exists a constant C such that

$$(B_{j-1/2}-F_{j-1/2})-(B_{j+1/2}-F_{j+1/2})\leqslant C. \tag{B.10}$$

Combining eqns (B.7), (B.8) and (B.10), we obtain

$$\|p^{n+1}\|_2 \leqslant \frac{1+(C/4)\Delta t}{1-(C/4)\Delta t}\|p^n\|_2. \qquad \text{(B.11)}$$

Therefore, the fully discretized method eqn (B.5) is stable.

Appendix C

C.1. DERIVATION OF THE ABSORBING BOUNDARY CONDITION

If the protein reaches an absorbing boundary, it is instantaneously removed from the system. Therefore, the probability of finding the protein at an absorbing boundary is zero. Suppose there is an absorbing boundary at $x = 0$ (at the left end of the computation domain). We must enforce the condition $\rho(0, t) = 0$.

To derive an appropriate jump rate for the absorbing boundary, we use the same procedures as we did in Appendix A. We first approximate eqn (A.1) in $[0, \Delta x]$ by

$$\frac{\partial \rho}{\partial t} = D\frac{\partial}{\partial x}\left(-\frac{f}{k_B T}\rho + \frac{\partial \rho}{\partial x}\right), \qquad \text{(C.1)}$$

where $f = -(\phi_1 - \phi_0)/\Delta x$ is an approximation for $-\partial\phi/\partial x$ in $(0, \Delta x)$. To derive a second-order treatment of the boundary, we only need a first-order approximation for this derivative.

As we argued in Appendix A, when Δx is small, the local structure of the solution is approximately given by the steady-state solution. At an absorbing boundary, the steady-state assumption in $(0, \Delta x)$ can also be justified mathematically by examining eqn (C.1) at $x = 0$. Because $\rho(0, t) = 0$, the left-hand side of eqn (C.1) is exactly zero at $x = 0$. Therefore, we set the left-hand side of eqn (C.1) to zero in the interval $(0, \Delta x)$ and solve the resulting ordinary differential equation subject to the following two conditions:

$$\rho(0) = 0, \qquad \text{(C.2)}$$

$$\int_0^{\Delta x} \rho(x)\,\mathrm{d}x = p_1. \qquad \text{(C.3)}$$

The solution is

$$\rho(x) = p_1 \frac{\exp(fx/k_B T) - 1}{(k_B T/f)[\exp(f\Delta x/k_B T) - 1] - \Delta x}. \qquad \text{(C.4)}$$

Using the above expression for $\rho(x)$, the flux is found to be

$$\begin{aligned} J &= D\frac{f}{k_B T}\rho - D\frac{\partial \rho}{\partial x} \\ &= -p_1 \frac{D}{(\Delta x)^2}\frac{\alpha^2}{\exp(\alpha) - 1 - \alpha}, \end{aligned}$$

$$\alpha = \frac{f\Delta x}{k_B T}. \qquad \text{(C.5)}$$

In the numerical scheme, the flux at the absorbing boundary is

$$J_{1/2} = -p_1 B_{1/2}^{absorb}. \qquad \text{(C.6)}$$

The above expression reflects the fact that once the protein reaches the absorbing boundary, it is removed from the system. Comparing eqn (C.5) with eqn (C.6), we get

$$\begin{aligned} B_{1/2}^{absorb} &= \frac{D}{(\Delta x)^2}\frac{\alpha^2}{\exp(\alpha) - 1 - \alpha}, \\ \alpha &= -\frac{\phi_1 - \phi_0}{k_B T}. \end{aligned} \qquad \text{(C.7)}$$

The equation for p_1 is then

$$\frac{\mathrm{d}p_1}{\mathrm{d}t} = -(B_{1/2}^{absorb} + F_{3/2})p_1 + B_{3/2}p_2. \qquad \text{(C.8)}$$

Similarly if an absorbing boundary is at $x = L$ (the right end of the computation domain), the equation for p_N is given by eqn (35) and $F_{N+1/2}^{absorb}$ is given by eqn (34).

Appendix D

D.1. THE STEADY-STATE DISTRIBUTION AND MEAN VELOCITY OF THE PERFECT BROWNIAN RATCHET

In this appendix, we show that for a loaded perfect ratchet (described in Section 3.2) our

numerical method yields the exact steady-state solution and thus the exact ratchet velocity. The steady-state solution of eqn (31) has the form

$$\rho(x) = c_1 \exp\left(\frac{fx}{k_B T}\right) + c_2. \tag{D.1}$$

At steady state, eqn (33) is satisfied automatically. Constants c_1 and c_2 are determined from eqn (32) and the requirement $\int_0^L \rho(x)\,\mathrm{d}x = 1$.

$$c_1 = -\frac{1}{L}\frac{\alpha_L \exp(-\alpha_L)}{\exp(-\alpha_L) - 1 + \alpha_L},$$

$$c_2 = \frac{1}{L}\frac{\alpha_L}{\exp(-\alpha_L) - 1 + \alpha_L}, \quad \alpha_L = \frac{fL}{k_B T}. \tag{D.2}$$

The probability flux is

$$J = D\left(\frac{f}{k_B T}\rho - \frac{\partial \rho}{\partial x}\right)$$

$$= \frac{D}{L^2}\frac{\alpha_L^2}{\exp(-\alpha_L) - 1 + \alpha_L}. \tag{D.3}$$

The average velocity of the ratchet is

$$v = LJ = \frac{D}{L}\frac{\alpha_L^2}{\exp(-\alpha_L) - 1 + \alpha_L},$$

$$\alpha_L = \frac{fL}{k_B T}. \tag{D.4}$$

In the spatial discretization, we divide $(0, L)$ into N sub-intervals of equal size ($\Delta x = L/N$). The site $x_n = (n - 1/2)\Delta x$ represents the sub-interval $((n-1)\Delta x, n\Delta x)$. Let ρ_n be the exact probability that the particle is in the interval $((n-1)\Delta x, n\Delta x)$. ρ_n is derived from the exact steady-state solution $\rho(x)$ given in eqns (D.1) and (D.2).

$$\rho_n = \int_{(n-1)\Delta x}^{n\Delta x} \rho(x)\,\mathrm{d}x. \tag{D.5}$$

To demonstrate that our numerical method yields the exact steady-state solution and the exact ratchet velocity for a perfect ratchet, we need to show that the exact probabilities $\{\rho_n\}$ satisfy the discrete equation with the correct probability flux:

$$F_{n+1/2}\rho_n - B_{n+1/2}\rho_{n+1}$$

$$= \frac{D}{L^2}\frac{\alpha_L^2}{\exp(-\alpha_L) - 1 + \alpha_L},$$

$$n = 1, \ldots, N-1, \tag{D.6}$$

$$F_{N+1/2}^{absorb}\rho_N = \frac{D}{L^2}\frac{\alpha_L^2}{\exp(-\alpha_L) - 1 + \alpha_L}, \tag{D.7}$$

where the jump rates are given by

$$F_{n+1/2} = \frac{D}{(\Delta x)^2}\frac{-\alpha}{\exp(-\alpha) - 1}, \quad \alpha = \frac{f\Delta x}{k_B T},$$

$$B_{n+1/2} = \frac{D}{(\Delta x)^2}\frac{\alpha}{\exp(\alpha) - 1},$$

$$F_{N+1/2}^{absorb} = \frac{D}{(\Delta x)^2}\frac{\alpha^2}{\exp(-\alpha) - 1 + \alpha}. \tag{D.8}$$

Equations (D.6) and (D.7) are found to be valid when we substitute eqns (D.1), (D.2), (D.5) and (D.8) into them. Thus, our numerical method yields the exact solution for a perfect ratchet.

Appendix E

E.1. CALCULATING INDIVIDUAL COMPONENTS OF THE DRIVING FORCE

The motor potential, in general, results from more than one interaction. For example, in models of the F_o motor, several proton binding sites on the rotor interact electrostatically with the membrane potential and with the stator charge (Elston *et al.*, 1998; Dimroth *et al.*, 1999). In order to examine the role of each interaction in the force generation, we need to design a method for calculating the contribution of a part of the motor potential to the driving force. This will allow us to identify the key interactions for the force generation. In this appendix, we develop the method for the simple case where a particle is driven by a constant force plus a periodic potential. The method developed can be applied to other situations.

We start with the governing equation

$$\frac{\partial \rho}{\partial t} = \frac{\partial}{\partial x}\left(D\frac{\phi'(x)}{k_B T}\rho + D\frac{\partial \rho}{\partial x}\right),$$

$$\phi(x) = \phi_p(x) - fx, \tag{E.1}$$

where $\phi_p(x)$ is a periodic potential with period L, and f is a constant force.

The spatial discretization is constructed with $\Delta x = L/N$ and $x_n = (n - 1/2)\Delta x$. In the derivation of jump rates (Appendix A), we showed that an approximate solution of eqn (E.1) in the interval $(x_{n-1/2}, x_{n+3/2})$ is

$$\rho(x) = c_1 \exp\left(\alpha \frac{x - x_{n+1/2}}{\Delta x}\right) + c_2,$$

$$c_1 = -\frac{\alpha \exp(\alpha)(p_n - p_{n+1})}{\Delta x\,(\exp(\alpha) - 1)^2},$$

$$c_2 = \frac{\exp(\alpha)p_n - p_{n+1}}{\Delta x\,(\exp(\alpha) - 1)}, \quad \alpha = \frac{-\Delta\phi_{n+1/2}}{k_B T}. \tag{E.2}$$

Suppose $\psi(x)$ is part of the potential $\phi(x)$. The contribution of $\psi(x)$ to the driving force is

$$\langle -\psi' \rangle = \int_0^L -\psi'(x)\rho(x)\,\mathrm{d}x. \tag{E.3}$$

We approximate $\psi'(x)$ at $x = x_{n+1/2}$ by the central difference and approximate $\psi'(x)$ in the interval $(x_{n-1/2}, x_{n+1/2})$ by a linear interpolation

$$\psi'(x_{n+1/2}) = \frac{\Delta\psi_{n+1/2}}{\Delta x},$$

$$\psi'(x) = \frac{\Delta\psi_{n+1/2}}{\Delta x}\left(\frac{x - x_{n-1/2}}{\Delta x}\right) + \frac{\Delta\psi_{n-1/2}}{\Delta x}\left(\frac{x_{n+1/2} - x}{\Delta x}\right). \tag{E.4}$$

Combining eqns (E.3), (E.4) and (E.2) yields

$$\begin{aligned}\langle -\psi' \rangle &= \sum_{n=1}^{N} \frac{-\Delta\psi_{n+1/2}}{\Delta x} \int_{x_{n-1/2}}^{x_{n+3/2}} \left(1 - \left|\frac{x - x_{n+1/2}}{\Delta x}\right|\right)\rho(x)\,\mathrm{d}x \\ &= \sum_{n=1}^{N} \frac{-\Delta\psi_{n+1/2}}{\Delta x} \int_{-1}^{1} \Delta x(1 - |s|)\,(c_1 \exp(\alpha s) + c_2)\,\mathrm{d}s.\end{aligned} \tag{E.5}$$

In the above expression, we have used the change of variables: $s = (x - x_{n+1/2})/\Delta x$. Substituting c_1 and c_2 into eqn (E.5), and integrating by parts, we obtain

$$\langle -\psi' \rangle = \sum_{n=1}^{N} \frac{-\Delta\psi_{n+1/2}}{\Delta x}\left(p_n \frac{\mathrm{e}^{-\alpha} - 1 + \alpha}{(-\alpha)(\mathrm{e}^{-\alpha} - 1)} + p_{n+1}\frac{\mathrm{e}^{\alpha} - 1 - \alpha}{\alpha(\mathrm{e}^{\alpha} - 1)}\right),$$

$$\alpha = \frac{-\Delta\phi_{n+1/2}}{k_B T} = \frac{-(\phi(x_{n+1}) - \phi(x_n))}{k_B T}. \tag{E.6}$$

Here we need to point out that in the above α varies with n and the complete notation should have been $\alpha_{n+1/2}$. Equation (E.6) has the following properties:

1. When the solution of eqn (E.1) is smooth, eqn (E.6) is second-order accurate for calculating $\langle -\psi' \rangle$.
2. Equation (E.6) is consistent with the numerical method in the sense that $\langle -\phi' \rangle$ calculated by eqn (E.6) is equal to the average driving force given by the numerical method ($= (k_B T/D)L$ flux).
3. When the solution of eqn (E.1) is discontinuous, eqn (E.6) is first-order accurate. This happens when the driving potential $\phi(x)$ is discontinuous, for example, the driving potential of a ratchet is a step function. Note that if we approximate eqn (E.3) by the trapezoidal rule, the resulting formula has no accuracy at all when the solution of eqn (E.1) is discontinuous.

Appendix F

F.1. IMPORTANCE OF DETAILED BALANCE

In this appendix, we show that numerical methods that do not respect detailed balance produce artificial velocities for systems at thermodynamic equilibrium.

When a system is at thermodynamic equilibrium, there is no energy consumption. The second law of thermodynamics dictates that the average velocity of the system should be zero. When a numerical method is applied to solve the equations of a system at thermodynamic equilibrium, the numerical solution may be different from the equilibrium solution given by Boltzmann's distribution. If the numerical method satisfies detailed balance, then the steady-state numerical solution will be the same as the equilibrium solution and the average velocity predicted from the numerical solution will be zero. If the numerical method does not obey detailed balance, the average velocity predicted from the numerical solution, in general, will be non-zero. Of course, if the potential is smooth the numerical average velocity will converge to zero (the true average velocity) as we reduce the discretization step size Δx. However, the motor potential may not be smooth, and even if it is smooth we may not be able to resolve it with large numbers of grid points in high-dimensional problems The artificial drift velocity violates the second law of thermodynamics, and we should prevent it from occurring in numerical solutions. That is why we enforce detailed balance exactly in our numerical method. In this appendix, we use the central difference method as an example to illustrate the artificial drift velocity resulting from not obeying detailed balance.

The central difference method for solving eqn (2) is derived by replacing spatial derivatives in eqn (2) with central differences:

$$\frac{\partial p_n}{\partial t} = \frac{D}{k_B T}\frac{1}{\Delta x}\left[\frac{\Delta\phi_{n+1/2}}{\Delta x}\left(\frac{p_{n+1}+p_n}{2}\right) - \frac{\Delta\phi_{n-1/2}}{\Delta x}\left(\frac{p_n+p_{n-1}}{2}\right)\right] + D\frac{1}{\Delta x}\left[\frac{p_{n+1}-p_n}{\Delta x} - \frac{p_n-p_{n-1}}{\Delta x}\right]. \quad \text{(F.1)}$$

The central difference method eqn (F.1) can be cast into the form of a jump process eqn (4), in which case the jump rates are given by

$$F^C_{n+1/2} = \frac{D}{(\Delta x)^2}\left(1 - \frac{\Delta\phi_{n+1/2}}{2k_B T}\right),$$

$$B^C_{n+1/2} = \frac{D}{(\Delta x)^2}\left(1 + \frac{\Delta\phi_{n+1/2}}{2k_B T}\right). \quad \text{(F.2)}$$

We apply the central difference method to solve numerically eqn (2) for two potentials. First, we use the discontinuous sawtooth potential

$$\phi_S(x) = A\left(\mathrm{mod}\left(\frac{2x}{L}+1, 2\right) - 1\right). \quad \text{(F.3)}$$

Next, we use the asymmetric potential $\phi_1(x)$ given in eqn (23), which is the first three Fourier modes of $\phi_S(x)$. For both potentials, we use $A = 2.5k_BT$, $L = 8$ nm and $D = 10^7$ nm^2 s^{-1}. In Fig. F1, the empty squares are the results for ϕ_S and filled circles are the results for ϕ_1. It is clear that the central difference method cannot handle discontinuous potentials. Although the

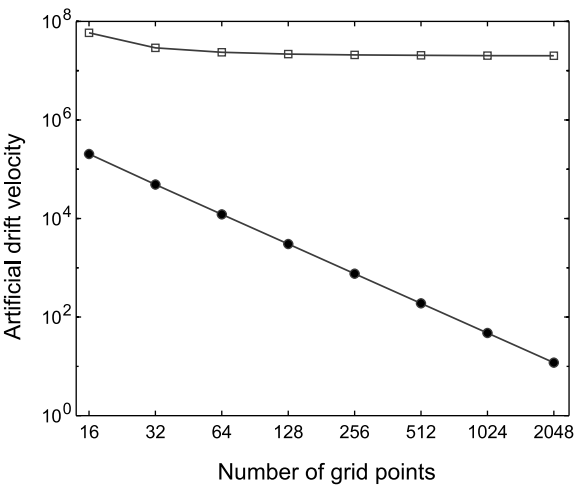

FIG. F1. The average velocity obtained with the central difference method vs. the number of grid points. The open squares are for the sawtooth potential and the closed circles are for the smooth approximation to this potential. For both potentials, the average velocity obtained with a numerical method obeying detailed balance will be zero (conforming to the second law of thermodynamics). The finite velocity shown is due to the fact that the central difference method does not obey detailed balance. For the smooth potential, this artificial velocity is proportional to Δx^2. For the sawtooth potential, the central difference method does not converge.

central difference is a second-order method, the artificial velocity for the discontinuous sawtooth potential does not decrease at all as Δx is reduced. For the smooth asymmetric potential ϕ_1, the artificial velocity behaves like $O((\Delta x)^2)$ as expected for a second-order method. However, to reduce the artificial velocity to 10 nm s^{-1}, we have to use more than 2000 points. This is computationally very expensive especially when dealing with two- or three-dimensional problems.

Appendix G

G.1. DERIVATION OF THE EQUATIONS FOR THE AVERAGE VELOCITY AND EFFECTIVE DIFFUSION COEFFICIENT

In this appendix we derive eqns (43) and (44) for the average velocity and effective diffusion equation. The derivation is an extension of the method used by Peskin & Oster (1995) to derive the effective diffusion coefficient for a model of kinesin. We start by defining the vector valued moments

$$\mathbf{m}_k = \sum_{j=-\infty}^{\infty} j^k \mathbf{p}(j,t). \tag{G.1}$$

Using eqn (41), one can derive a hierarchy of differential equations for these moments. The first three come out to be

$$\frac{\mathrm{d}\mathbf{m}_0}{\mathrm{d}t} = \mathbf{M}\mathbf{m}_0, \tag{G.2}$$

$$\frac{\mathrm{d}\mathbf{m}_1}{\mathrm{d}t} = \mathbf{M}\mathbf{m}_1 + (\mathbf{L}_+ - \mathbf{L}_-)\mathbf{m}_0, \tag{G.3}$$

$$\frac{\mathrm{d}\mathbf{m}_2}{\mathrm{d}t} = \mathbf{M}\mathbf{m}_2 + 2(\mathbf{L}_+ - \mathbf{L}_-)\mathbf{m}_1 + (\mathbf{L}_+ + \mathbf{L}_-)\mathbf{m}_0, \tag{G.4}$$

where $\mathbf{M} = \mathbf{L} + \mathbf{L}_+ + \mathbf{L}_-$. It is convenient to assume that eqn (G.2) is already at steady state. That is, that $\mathbf{m}_0 = \mathbf{p}^s$ is a constant vector satisfying the equation $\mathbf{M}\mathbf{m}_0 = 0$ subject to the normalization condition $\mathbf{1}\cdot\mathbf{p}^s = 1$, where $\mathbf{1}$ is the left zero eigenvector of the matrix $\mathbf{M}$ (i.e. $\mathbf{1}$ is a row vector of ones with dimension equal to the number of grid points). Taking the inner product of both sides of eqns (G.3) and (G.4) with respect to $\mathbf{1}$ produces

$$\frac{\mathrm{d}}{\mathrm{d}t}(\mathbf{1}\cdot\mathbf{m}_1) = \mathbf{1}\cdot(\mathbf{L}_+ - \mathbf{L}_-)\mathbf{p}^s, \tag{G.5}$$

$$\frac{\mathrm{d}}{\mathrm{d}t}(\mathbf{1}\cdot\mathbf{m}_2) = 2\mathbf{1}\cdot(\mathbf{L}_+ - \mathbf{L}_-)\mathbf{m}_1 + \mathbf{1}\cdot(\mathbf{L}_+ + \mathbf{L}_-)\mathbf{p}^s. \tag{G.6}$$

If we multiply eqn (G.5) by L, the period of the potential $\phi(x)$, we arrive at eqn (43) for the average velocity.

The equation we need to evaluate to get an expression for the effective diffusion coefficient is

$$\frac{\mathrm{d}}{\mathrm{d}t}[\mathbf{1}\cdot\mathbf{m}_2 - (\mathbf{1}\cdot\mathbf{m}_1)^2] = 2\mathbf{1}\cdot(\mathbf{L}_+ - \mathbf{L}_-)\mathbf{q} + \mathbf{1}\cdot(\mathbf{L}_+ + \mathbf{L}_-)\mathbf{p}^s, \tag{G.7}$$

where we have introduced the definition

$$\mathbf{q} = \mathbf{m}_1 - (\mathbf{1}\cdot\mathbf{m}_1)\mathbf{p}^s. \tag{G.8}$$

Note that $\mathbf{1}\cdot\mathbf{q} = 0$. We need to find the limit of $\mathbf{q}$ as $t\to\infty$. This is done by noting that $\mathbf{q}$ satisfies the differential equation

$$\frac{\mathrm{d}\mathbf{q}}{\mathrm{d}t} = \mathbf{M}\mathbf{q} - \mathbf{b}, \tag{G.9}$$

where $\mathbf{b}$ is the constant vector

$$\mathbf{b} = [\mathbf{1}\cdot(\mathbf{L}_+ - \mathbf{L}_-)\mathbf{p}^s]\mathbf{p}^s - (\mathbf{L}_+ - \mathbf{L}_-)\mathbf{p}^s. \tag{G.10}$$

Because $\mathbf{1}\cdot\mathbf{b} = 0$, a steady-state solution to eqn (G.10) exists and is determined by the equation

$$\mathbf{M}\mathbf{r} = \mathbf{b} \tag{G.11}$$

subject to the constraint $\mathbf{1}\cdot\mathbf{r} = 0$. The stability of this solution is determined by the non-zero eigenvalues of $\mathbf{M}$. Because $\mathbf{M}$ is a transition matrix all its eigenvalues are $\leqslant 0$. Therefore, $\mathbf{r}$ is a stable fixed point and all solutions of eqn (G.9) asymptotically approach this solution as $t\to\infty$. Therefore in the limit $t\to\infty$, eqn (G.7) for the variance becomes

$$\frac{\mathrm{d}}{\mathrm{d}t}[\mathbf{1}\cdot\mathbf{m}_2 - (\mathbf{1}\cdot\mathbf{m}_1)^2] = 2\mathbf{1}\cdot(\mathbf{L}_+ - \mathbf{L}_-)\mathbf{r} + \mathbf{1}\cdot(\mathbf{L}_+\mathbf{L}_-)\mathbf{p}^s, \tag{G.12}$$

where

$$\mathbf{Mr} = [\mathbf{1} \cdot (\mathbf{L}_+ - \mathbf{L}_-)\mathbf{p}^s]\mathbf{p}^s - (\mathbf{L}_+ - \mathbf{L}_-)\mathbf{p}^s \quad \text{(G.13)}$$

subject to the constraint $\mathbf{1} \cdot \mathbf{r} = 0$. Noting that

$$D_{eff} = \frac{L^2}{2}\frac{\mathrm{d}}{\mathrm{d}t}[\mathbf{1} \cdot \mathbf{m}_2 - (\mathbf{1} \cdot \mathbf{m}_1)^2] \quad \text{(G.14)}$$

produces eqn (44) of the text.

We note that examining only the first two moments does not guarantee the process is Gaussian. However, using the probability generating function, it is possible to show that the process becomes normal in the long time limit (Elston, 2000). The probability generating function approach can also be used to derive the equations for average velocity and effective diffusion coefficient.